HHS Public Access

Author manuscript

J Magn Reson Imaging. Author manuscript; available in PMC 2019 June 01.

Published in final edited form as:

J Magn Reson Imaging. 2018 June ; 47(6): 1667–1676. doi:10.1002/jmri.25893.

Measuring human placental blood flow with multi-delay 3D GRASE pseudo-continuous arterial spin labeling at 3 Tesla

Xingfeng Shao, MS[1], **Dapeng Liu, PhD**[2], **Thomas Martin, BS**[2], **Teresa Chanlaw, MPH**[3], **Sherin U. Devaskar, MD**[3], **Carla Janzen, MD**[4], **Aisling M. Murphy, MD**[4], **Daniel Margolis, MD**[2], **Kyunghyun Sung, PhD**[2,*], and **Danny JJ Wang, PhD, MSCE**[1]

[1]Laboratory of FMRI Technology (LOFT), Mark & Mary Stevens Neuroimaging and Informatics Institute, Keck School of Medicine, University of Southern California

[2]Department of Radiology, David Geffen School of Medicine at UCLA

[3]Department of Pediatrics, David Geffen School of Medicine at UCLA

[4]Department of Obstetrics and Gynecology, Division of Maternal Fetal Medicine, David Geffen School of Medicine at UCLA

Abstract

Background—Placenta influences the health of both a woman and her fetus during pregnancy. Maternal blood supply to placenta can be measured non-invasively using arterial spin labeling (ASL).

Purpose—To present a multi-delay pseudo-continuous arterial spin labeling (pCASL) combined with a fast 3D inner-volume Gradient-and Spin Echo (GRASE) imaging technique to simultaneously measure placental blood flow (PBF) and arterial transit time (ATT), and to study PBF and ATT evolution with gestational age during the second trimester. The PBF values were compared with uterine arterial Doppler ultrasound to assess its potential clinical utility.

Study type—This was a prospective study.

Subjects—Thirty-four pregnant women.

Field Strength/Sequence—Multi-delay 3D inner-volume GRASE pCASL sequence on 3T MR scanners.

Assessment—Subjects underwent two longitudinal MRI scans within the second trimester, conducted between 14–16 and 19–22 weeks of gestational age, respectively. Placental perfusion was measured using the free-breathing pCASL sequence at three post-labeling delays (PLDs), followed by offline motion correction and model fitting for estimation of PBF and ATT.

Statistical Tests—Paired t-test was conducted to evaluate the significance of PBF/ATT variations with placental development. Two-sample t-test was conducted to evaluate the significance of PBF difference in subjects with and without early diastolic notch.

[*]**Corresponding Author:** Kyunghyun Sung, PhD, Address: 300 UCLA Medical Plaza, Suite B119, Los Angeles, CA 90095-7350, Phone: 310-267-6842, Fax: 310-825-9118, ksung@mednet.ucla.edu.

Results—The mean PBF and ATT for the second trimester were 111.4±26.7 ml/100g/min and 1387.5±88.0 ms respectively. The average PBF increased by 10.4% (P<0.05) while no significant change in ATT (P=0.72) was found along gestational ages during the second trimester. PBF decreased 20.3% (P<0.01) in subjects with early diastolic notches in ultrasound flow waveform patterns.

Data Conclusion—Multi-delay pCASL with inner-volume 3D GRASE is promising for noninvasive assessment of PBF during pregnancy. Its clinical use for the detection of aberrations in placental function and prediction of fetal developmental disorders awaits evaluation.

Keywords

Placental blood flow (PBF); Arterial spin labeling (ASL); Gestational age; Human placenta; Magnetic resonance imaging (MRI)

INTRODUCTION

Placenta supports the pregnancy by providing the developing fetus with nutrients and oxygen via maternal blood supply. Maternal blood enters the placenta through the spiral arteries and perfuse intervillous spaces. Exchange of oxygen and nutrients with fetal blood occurs when maternal blood flows around the villi (1). Placental perfusion depends on both maternal blood supply and resistance of placenta to blood flow. Pathological development of the utero-placental unit or defective trophoblastic invasion, which can lead to intrauterine growth restriction (IUGR) and Pre-eclampsia (PE), increases the resistance of the spiral arteries or placenta vascular bed to blood flow, and restricts placental perfusion (2).

Uterine artery Doppler ultrasound, which is a routine approach for prenatal examination, has been widely applied to measure blood flow through utero-placental circulation non-invasively due to its low-cost and high temporal resolution. Doppler ultrasound assesses placental perfusion through measuring impedance to flow in the uterine arteries, which has been reported to be increased in pregnancies with PE or IUGR (3). However, Doppler ultrasound measurements of placental perfusion lack sufficient reproducibility and sensitivity, and quantification remains challenging (4).

In contrast, magnetic resonance imaging (MRI) produces spatially resolved perfusion images and quantitative assessment. Perfusion MRI is typically measured by three common approaches: First of which manipulates blood relaxation time by injecting contrast agents, which has been precluded for use during pregnancy in the United States due to the concerns of deposition of Gadolinium (Gd) in tissues (5). Alternatively, placenta perfusion has been successfully measured by two non-invasive approaches: intra-voxel incoherent motion (IVIM) and arterial spin labeling (ASL). The IVIM technique acquires diffusion weighted images with multiple b-values and calculates perfusion fraction by fitting a two-compartment model, considering placental perfusion as a fast pseudo-diffusion process due to pseudo-random capillary blood flow (6). The ASL technique labels water molecules in arterial blood using radiofrequency (RF) pulses and magnetic gradients without introducing any radiation. First ASL study in placenta was conducted by Gowland using flow-sensitive alternating inversion recovery (FAIR) ASL, which compares the magnetization in the

imaging region following non-selective and selective inversion pulses and has been implemented in a number of studies to non-invasively determine placental perfusion (6–8). However, both IVIM and FAIR ASL techniques measure the movement of blood within the placenta containing both maternal and fetal flow, which are around 600 ml/min and 360 ml/min at term, respectively (9). As a result, an overestimation of placental perfusion complicates the understanding of maternal blood supply. Additional, relatively low signal-to-noise ratio (SNR) of single-slice FAIR ASL requires lengthy measurements and is susceptible to motion artifacts.

As an alternative, pseudo-continuous ASL (pCASL), which employs a train of discrete RF pulses to mimic flow-driven adiabatic inversion, is capable of selectively labeling maternal feeding aorta and distinguishing the source of perfusion. Compared to FAIR ASL, superior SNR has resulted in growing applications of pCASL perfusion for other body organs, such as kidney and liver (10,11). The purpose of this study was to present a multi-delay pCASL sequence combined with a fast 3D inner-volume Gradient-and Spin Echo (GRASE) imaging technique for non-invasive and simultaneous assessment of placental blood flow (PBF) and arterial transit time (ATT) in pregnant women. Potentially, this work facilitates the goals of the Human Placental Project to develop non-invasive imaging techniques to understand placental development and function in real time (12).

METHODS

MR Pulse Sequence Design

Figure 1 (a) shows the diagram of pCASL GRASE sequence with background suppression and inner volume excitation. Background suppression was applied to minimize temporal fluctuations due to motion and other system instabilities using two inversion pulses and a pre-saturation pulse (13). Inversion pulses were inserted within the post-labeling delay (PLD) and the timing was optimized using a custom Matlab program, as described in (14), to null/minimize uterine tissue signal at excitation for T1 values ranging from 1400 to 1700ms with a step size of 25ms (15). Inner volume excitation was achieved by switching the slice-selective gradient to phase encoding (PE)-axis for re-focusing pulses (16). Only imaging volume within the intersection of two perpendicular selective bands (slice and PE directions) was refocused after excitation and image overlap due to limited field-of-view (FOV) along PE direction was avoided. Inner-volume excitation also enabled single-shot GRASE readout to cover the placenta, which further improved the robustness of the sequence to motion. Fat saturation was inserted before the excitation pulse of GRASE readout using an excitatory frequency selective RF pulse followed by a strong spoiler gradient along Y-axis.

Three-plane T2 weighted Half-Fourier Acquisition Single-shot Turbo spin Echo (HASTE) images were acquired before ASL scan to assist the positioning of the labeling plane and imaging volume (17). Figure 1 (b) shows the coronal and sagittal view of experimental setup. The imaging volume was selected as perpendicular to the maternal-fetal axis and to cover as much of placenta as possible. The labeling plane was placed proximal perpendicular to the abdominal aorta and above the aortic bifurcation through a graphic user interface (GUI).

Simulation of Labeling Efficiency

Bloch equation simulations were performed to estimate the labeling efficiency at the aortic bifurcation using the numerical integration proposed in (18). Parameters of the pCASL scheme were: Hanning window-shaped RF pulse with duration/space 500 us/920 us, flip angle = 25°, slice-selective gradient = 6 mT/m and average gradient = 0.6 mT/m. The average slew rate of switching slice-selective gradient was 88.4 mT/m/ms, which was kept below 50% of maximum (200 mT/m/ms) to reduce noise exposure. T1 and T2 relaxation time for arterial blood at 3T were assumed to be 1660 and 100 ms, respectively (19).

Due to relatively high distal resistance and capacitance of the arteries in the lower limbs, blood flow waveform at aortic bifurcation becomes tri-phasic: starting with a strong forward flow phase in peak systole ($v < 23$ cm/s) followed by a negative flow phase in early diastole ($v < 13$ cm/s) and a slower forward flow phase in late diastole ($v < 15$ cm/s) (20). To simplify simulation, net flow in diastole stage was assumed to be zero since the velocity distribution was similar in phase 2 and 3 despite the opposite sign. Thus, blood flow velocity of 11.5 cm/s, a half of flow velocity at peak systole, was used to represent the mean velocity through whole cardiac phase. Cross-sectional velocity distribution was assumed to be parabolic, corresponding to laminar flow, and labeling efficiency was calculated as the weighted average for velocities ranging from 0 (vessel wall) to 11.5 cm/s (vessel center), as described in (18). To compare the labeling efficiency at carotid, where the labeling label is placed for cerebral blood flow measurement, Bloch equation simulation was conducted for vessel center velocity = 11.5 cm/s and 40.3 cm/s, respectively (21).

MRI Experiments

A total of 34 normal pregnant women (age = 32.6±4.5 years) were scanned on Siemens 3T scanners (Prisma and Skyra; Siemens Healthcare, Erlangen, Germany) after they provided informed consent according to a protocol approved by the local Institutional Review Board (IRB). Each subject was scanned twice within the second trimester, where the first and second MRI scans were conducted between 14–16 weeks and 19–22 weeks of gestational age, respectively. Placental perfusion was measured using the single-shot 3D pCASL at three PLDs: 1000, 1500 and 2000 ms. Imaging parameters were: FOV=300, eight slices with 20% slice oversampling, single shot, matrix=96×96, resolution=3.1×3.1×3mm^3, bandwidth=2604Hz/pixel, echo spacing=0.49ms, TE=36.5ms, TR=4000ms, label/control duration=1500ms, each PLD contained 14 repetitions and one M0 scan with a total scan time of 2min 4sec. Global specific absorption rate (SAR) was measured at each MRI scan to monitor RF heating. Subjects were instructed to relax and breath normally during the entire scan period.

Data Analysis

Control/label images were corrected for non-rigid body motion off-line using ANTs (Advanced Normalization Tools: http://www.picsl.upenn.edu/ANTS), which deforms the image time series towards a target image using a cross-correlation-based symmetric diffeomorphic transformation (22). Perfusion images were obtained through the subtraction of the control/label images. Outliers of the perfusion images were removed when identified as beyond two standard deviations. Temporal fluctuations in the difference image series

owing to residual motion and physiologic noise were minimized using an algorithm based on principal component analysis (23). Perfusion signal was measured in hand-drawn region of interest (ROI) based on T2 weighted GRASE control images. Pixel-wise PBF was estimated based on the following equation, as described in (24):

$$f = \frac{\Delta M \lambda R_{1a}}{2\alpha M_0 \left[\exp\left((\min(\delta - w, 0) - \delta) R_{1a}\right) - \exp\left(-(\tau + w) R_{1a}\right)\right]}, \quad [1]$$

where ΔM is the averaged signal difference after pair-wise subtraction (control-label), M_0 is the equilibrium magnetization, f is blood flow, α is the labeling efficiency of pCASL scheme. As a highly-vascularized organ, the blood and placental tissue water partition coefficient λ was assumed to be 1 ml/g (7), is PLD, τ is labeling duration, R_{1a} (1/1660 ms^{-1}) is the longitudinal relaxation rate of blood (25), δ is the transit time from the labeling region to the tissue compartment, min(x_1, x_2) function returns the smaller value of x_1 and x_2.

Arterial transit time (ATT), δ, was calculated based on a monotonic relationship with weighted delay (WD), which was calculated from perfusion signals (ΔM_i) at multiple PLDs (26):

$$WD = \left(\sum_{i=1}^{N} w_i \Delta M_i\right) / \left(\sum_{i=1}^{N} \Delta M_i\right) \quad [2]$$

where N is the number of PLDs and N=3 in the current study (w_i=1,1.5,2s). The weighted delay approach has been shown to be robust for ATT estimation with a few sample points (24) and methodological details were explained in supplemental Figure 1. PBFs (f_i) were then calculated for each PLD based on Equation [1] that incorporated estimated ATT, and averaged to produce the final mean PBF.

Temporal SNR (t-SNR) was calculated as the ratio of the mean signal to the standard deviation (SD) of the perfusion time series for each PLD. Pixel-wise PBF, ATT and t-SNR were averaged for each subject within hand-drawn ROIs, which covered most of the placenta volumes and were drawn by two research fellows based on T2 weighted GRASE control images. Repeated scans from 34 subjects were analyzed for PBF and ATT variations with placental development. Mean and SD of PBF and ATT values were calculated for each scan across all participants respectively.

Histogram analysis was conducted by dividing the range of PBF values into 9 consecutive bins with a width of 50 ml/100g/min except an open-ended bin at last. Fraction of PBF values in each bin was averaged across 34 subjects at repeated scans. Placenta volume was classified into 9 regions corresponding to bins of PBF values, and mean ATT in each region averaged from all subjects at repeated scans.

Uterine Arterial Doppler Ultrasound Acquisitions

The PBF values were compared with uterine arterial Doppler ultrasound measurement to assess its potential clinical utility. Bilateral uterine arterial Doppler ultrasound was collected from 21 and 20 subjects using a GE Voluson 830 expert system (GE Medical Systems, Zipf, Austria) after they received the first and second MRI scans, respectively (16 subjects had ultrasound after both MRI scans). RI (resistive index; difference between systolic and diastolic velocity divided by systolic velocity), PI (pulsatility index; difference between systolic and diastolic velocity divided by time averaged velocity), and notching at early diastole were measured on both left and right uterine arteries. Poor placental perfusion is typically indicated by increased RI, PI or the persistence of an early diastolic notch in uterine blood flow waveform pattern, which is caused by a reflected wave returning from uteroplacental bed due to high vascular resistance.

Statistical Analysis

Average PBF and ATT were calculated for each subject and compared between the repeated MRI scans. Paired t-test was conducted to evaluate the significance of PBF/ATT variations with placental development. RI and PI were correlated with average PBF using linear regression. Two-sample t-test was conducted to evaluate the significance of PBF difference in subjects with and without early diastolic notch. All statistical analysis was performed in Matlab (Mathworks Inc, Natick, MA, USA) and $P<0.05$ (2-tailed) was considered as significant.

RESULTS

Figure 2 (a) shows the simulated time courses of longitudinal magnetization (Mz) of spins flowing across the labeling plane with v = 11.5 (aortic bifurcation) and 40.3 cm/s (carotid artery) under the label condition. Mz experiences inversion when spin approaches the labeling plane, and then recovers following T1 relaxation. The control condition caused a small perturbation of Mz (<3%) as shown in Figure 2 (b). Labeling efficiency were 77.2% and 92.1% for v = 11.5 and 40.3 cm/s, respectively, after correcting the measured efficiency at t = 1000 ms for the T1 recovery experienced in transit from the tagging plane. The labeling efficiency was averaged to be 63.8% for laminar flow at aortic bifurcation, which was used to estimate PBF in the current study. In our study, the global SAR was averaged to be 1.19±0.23 W/kg.

Placental Perfusion

Perfusion signals measured at three PLDs reveal the dynamic course of labeled blood flowing through the placenta. Figure 3 (a) shows one slice of perfusion images (overlaid on T2-weighted structural image) acquired at three PLDs from one representative subject. Calculated PBF and ATT maps are shown in figure 3 (b) and (c) respectively. As expected, perfusion signal decays with longer PLDs due to the T1 relaxation within the majority of placental areas, while spatial variation of perfusion signal with focal hyperintensities can also be observed, as indicated by a blue arrow in PBF map. Spatial heterogeneity of perfusion signals indicates potential spatial variation in the vascular structure of the placenta,

which is not seen in T2-weighted images. Mean t-SNR across 34 subjects were 1.39±0.05, 1.40±0.13 and 1.42±0.15 at PLD= 1000, 1500 and 2000 ms, respectively.

Figure 4 shows 3D view of PBF (a) and ATT (b) maps covering the whole placenta volume from the same subject as shown in Figure 3. According to the weighted delay approach, ATT values shorter than 1000 ms or greater than 2000 ms cannot be estimated due to the range of selected PLDs, as shown in Figure 3 (b). Three coronal/sagittal images with apparent hyper-perfusion regions are displayed next to the transversal image to show those regions in 3D view. The spatial locations of the hyper-perfusion regions are highlighted by arrows in the transversal plane.

PBF/ATT Change Along Pregnancy

As illustrated in Figure 5, PBF/ATT values of the second scan (19–22 weeks) are plotted against the values acquired at the first scan (14–16 weeks). The average PBF increased by 10.4% ($P<0.05$) while no significant change in ATT ($P=0.72$) along gestational age. Mean and SD of PBF and ATT values are summarized in Table 1. Overall, PBF and ATT for the second trimester were 111.4±26.7 ml/100g/min and 1387.5±88.0 ms respectively.

Figure 6 (a) shows the fraction of PBF values in 9 consecutive bins at repeated scans. The 1st and 2nd scan had 3.5% and 3.6% regions with high PBF values (≥300 ml/100g/min), respectively, while the 1st scan appeared to have 8.9% more regions with lower perfusion rate (0–100 ml/100g/min). Figure 6 (b) showed the mean ATT in each region averaged from all subjects at repeated scans. ATT increased in regions with high PBF values, which is consistent with the observation that perfusion signal peaked at late PLD in focal hyper-perfusion regions, as shown in Figure 3 (a).

Comparision Between PBF and Ultrasound Results

Scatter plot of PI and RI against average PBF was shown in Figure 7. No significant correlation between PI/RI and PBF was found in this study and *P* values were listed next to each dashed line in Figure 7. Subjects with early diastolic notch were labeled by red filled marks (squares and triangles) in Figure 7. Notches presented in four subjects' Doppler ultrasound waveform pattern acquired after the first MRI scan, while two subjects had persistent notches at both measurements, as identified by blue and green arrows in Figure 7. Average PBF across subjects with unilateral or bilateral notch is 89.1±12.4 ml/100g/min, which is significantly lower than 111.9±22.4 ml/100g/min averaged from the subjects without notch ($P<0.01$). A 20.3% reduction in PBF is consistent with the presence of notches in the waveform pattern, which represents the sign of high impedance to flow (27).

DISCUSSION

The first human placental ASL imaging was reported by Gowland and her colleagues at 0.5 T (mean±SD PBF=176±24 ml/100g/min) using FAIR ASL with a total of 20 pairs of control/label images acquired at 10 inversion times (7). Since then, FAIR ASL has been adopted in a number of studies, and one of which reported reduced placental perfusion in the pregnancies that resulted in Small-for-Gestational-Age (SGA) neonates (6). Compared to previous studies, our experiments were conducted on 3T scanners and multi-slice images

were acquired using pCASL with single shot 3D acquisition. Both improvements led to significant SNR increase, which is beneficial for clinical scans when time is limited. The spatially resolved visualization of placental perfusion indicated heterogeneity of perfusion signals within the placenta. Heterogeneity of placental perfusion has been previously reported using single slice FAIR ASL (7,8), velocity-selective ASL (28) and BOLD fMRI (29). The origin of this perfusion heterogeneity is not well understood but was assumed to be related to the underlying vascular units, i.e. cotyledons, of the placenta. With perfusion signals acquired at three delay times, it is feasible to perform dynamic analysis of regions of interest to better understand how labeled blood passes through the placenta.

Background suppression, which is recommended by ASL white paper (13), is ideally suited for GRASE readout and helps suppress temporal fluctuations from motion and systematic instabilities. A constrained background suppression scheme, which applied non-selective inversion pulses within the PLD, was implemented for this study to keep the labeling scheme intact. Though placenta was reported to have longer T1 values than the 1400–1700 ms optimization range used in this study (30), similar background suppression effect is achievable for PLDs from 1000 to 2000 ms, as reported in our previous research (14). To ensure the accuracy for ATT estimation, the labeling plane was placed at the aortic bifurcation, which is easy to identify compared to tortuous uterine arteries, by trained MR technicians and research fellows. Transit time of arterial blood from labeling plane to the majority of placenta was assumed to be shorter than 2 sec due to the relative high blood velocity in uterine arteries (mean velocity > 70 cm/s around 20 weeks of gestation) (31).

All pregnant subjects were scanned within their second trimester when fetal movement becomes more strenuous in late pregnancy potentially causing severe motion artifacts in perfusion images. Averaged PBF value was 111.4±26.7 ml/100g/min for the second trimester, which is consistent with but at the lower end of reported PBF values (7,8,28). This is expected since pCASL selectively labeled maternal perfusion of placenta. Additionally, the maternal blood supply and the mass of placenta have been reported to be around 600 ml/min and 550 g at term, respectively (7,9), so that approximate placenta perfusion rate should be around 110 ml/100g/min, which is highly consistent with our results. Additionally, we found a 20.3% reduction in PBF from subjects with early diastolic notches in ultrasound flow waveform patterns as compared to subjects without notches, which indicates high resistance to blood flow. Since ultrasound is an established imaging modality, this result supports the validity of the presented ASL approach for assessing placental function. Since ASL is completely noninvasive, repeated scans can be acquired from the same pregnant subject, allowing quantitative analysis for PBF and ATT variations along placental development within the second trimester. Significant increase in placental perfusion during the second trimester was observed from 34 subjects in our study, which is consistent with previous ultrasound studies demonstrating increase of total uterine artery blood flow around 20 weeks of pregnancy (31). Nevertheless, whole placenta PBF maps provide spatially resolved diagnostic information than average PBF values of the whole placenta, which provides an understanding of the underlying vascular structure and potential pathological changes associated with observed perfusion variation. Such information is particularly useful for building prediction models towards projecting a clinical outcome in the future. In addition, under circumstances where blood flow to the placenta is abnormal, future

correlation with conditions of placental insufficiency as a pregnancy progresses may prove to be a valuable as a diagnostic tool.

Many studies reported no known adverse effects of using non-contrast MRI during pregnancy (32,33). In our study, the global SAR was 1.19±0.23 W/kg, about 60% of the FDA normal mode limit. Although monitoring the global SAR is sufficient for ensuring RF heating at 3T or less, the local SAR simulation may need to be conducted for other setups (34). Another safety concern includes the acoustic noise induced by switching gradients. Maternal tissue provides inherent protection to fetal hearing by an approximate 30-dB reduction in sound intensity (35). A variety of fast imaging sequences, including echo-planar imaging (EPI) and fast spin echo (FSE), have been tested at 1.5 T, and no association between acoustic noise and increased risk of substantial neonatal hearing impairment or cochlear injury was found (36). Although 3T scanners would generate higher noise level compared to 1.5T (37), duration of the exposure is more important and occupational health guidelines stipulate that exposure to acoustic noise greater than 115 dB should be restricted to less than 15 minutes per day (US Department of Labor, Occupational Safety and Health Administration. Regulations (Standards - 29 CFR). Part 1910.95: occupational noise exposure.). Both RF heating effects and acoustic noise exposure were minimized due to the relative short ASL scan time (about 6 mins) used in this study.

The inner-volume excitation allowed single-shot GRASE readout to cover the entire placenta in 8 slices. This improved the robustness of the sequence to motion. Non-rigid motion correction has also been proven to be beneficial for body ASL imaging (11), and 14 control volumes from a representative subject acquired at PLD=1000 ms with and without non-rigid motion correction was shown in supporting video 1. Deviation from perfect inversion occurred for slow spins at aortic bifurcation due to suboptimal adiabatic condition (38), and the pCASL labeling parameters (RF flip angle and gradient strength) may be optimized based on aortic flow velocity profiles to improve the labeling efficiency for placental perfusion imaging. Chemical shift would not contaminate ASL signal when subtraction is perfect, but displaced fat signal between control/label pairs could introduce artifacts to perfusion images. Fat suppression was applied before GRASE readout in this study but residual fat signal was still observed, compared to background suppressed tissue signal in several subjects. Thus, further improvement of fat suppression is desirable to improve SNR. In addition, limited portability and high cost of MRI may constraint its capability of being a routine prenatal examination approach, as compared to Doppler ultrasound.

The study includes several limitations. First, the motion from respiration and feta movement was the major limitation of reliable PBF measurements using ASL. The PBF measurement in late gestational age may require additional motion compensation for more reliable measurements. Second, the sample size of the study was relatively small, and not all subjects had ultrasound examinations. Future studies with a larger sample size are required to replicate the reported association between PBF and ultrasound as well as to investigate the relationship between PBF and clinical outcomes of pregnancy. Third, the placenta perfusion heterogeneity was not fully understood. Dynamic analysis of perfusion signals may be needed to further understand how the labeled blood passes through the placenta. In addition,

the correlation between in-vivo placenta perfusion and pathological analysis of the placenta may help understand the origin of the perfusion heterogeneity.

In conlusion, we present a multi-delay pCASL sequence with inner-volume 3D GRASE acquisition, which is promising for non-invasive measurement of PBF and ATT during early- to mid-pregnancy. Its clinical use for the detection of aberrations in placental function and prediction of fetal developmental disorders awaits further evaluation.

Supplementary Material

Refer to Web version on PubMed Central for supplementary material.

Acknowledgments

Grant support: This work was funded by NIH U01-HD087221.

References

1. Wang Y, Zhao S. Vascular Biology of the Placenta, Integrated Systems Physiology: from Molecules to Function to Disease0. San Rafael (CA). 2010
2. Sibai B, Dekker G, Kupferminc M. Pre-eclampsia. Lancet. 2005; 365(9461):785–799. [PubMed: 15733721]
3. Campbell S, Diaz-Recasens J, Griffin DR, et al. New doppler technique for assessing uteroplacental blood flow. Lancet. 1983; 1(8326 Pt 1):675–677. [PubMed: 6132039]
4. Lai PK, Wang YA, Welsh AW. Reproducibility of regional placental vascularity/perfusion measurement using 3D power Doppler. Ultrasound Obstet Gynecol. 2010; 36(2):202–209. [PubMed: 20201118]
5. Salomon LJ, Siauve N, Balvay D, et al. Placental perfusion MR imaging with contrast agents in a mouse model. Radiology. 2005; 235(1):73–80. [PubMed: 15695621]
6. Derwig I, Lythgoe DJ, Barker GJ, et al. Association of placental perfusion, as assessed by magnetic resonance imaging and uterine artery Doppler ultrasound, and its relationship to pregnancy outcome. Placenta. 2013; 34(10):885–891. [PubMed: 23937958]
7. Gowland PA, Francis ST, Duncan KR, et al. In vivo perfusion measurements in the human placenta using echo planar imaging at 0.5 T. Magn Reson Med. 1998; 40(3):467–473. [PubMed: 9727951]
8. Morris, DM., Wright, C., Dobbs, MS., et al. Arterial Spin Labelling in the Human Placenta – Mapping Perfusion. International Society for Magnetic Resonance in Medicine; 2012. p. 570
9. Moore P, Cooper G. Placental blood flow. Current Anaesthesia & Critical Care. 1999; 10(2):83–86.
10. Artz NS, Sadowski EA, Wentland AL, et al. Arterial spin labeling MRI for assessment of perfusion in native and transplanted kidneys. Magn Reson Imaging. 2011; 29(1):74–82. [PubMed: 20850241]
11. Pan X, Qian T, Fernandez-Seara MA, et al. Quantification of liver perfusion using multidelay pseudocontinuous arterial spin labeling. J Magn Reson Imaging. 2016; 43(5):1046–1054. [PubMed: 26445928]
12. Guttmacher AE, Maddox YT, Spong CY. The Human Placenta Project: placental structure, development, and function in real time. Placenta. 2014; 35(5):303–304. [PubMed: 24661567]
13. Alsop DC, Detre JA, Golay X, et al. Recommended implementation of arterial spin-labeled perfusion MRI for clinical applications: A consensus of the ISMRM perfusion study group and the European consortium for ASL in dementia. Magn Reson Med. 2015; 73(1):102–116. [PubMed: 24715426]
14. Shao X, Wang Y, Moeller S, Wang DJ. A constrained slice-dependent background suppression scheme for simultaneous multislice pseudo-continuous arterial spin labeling. Magn Reson Med. 2017

15. de Bazelaire CM, Duhamel GD, Rofsky NM, Alsop DC. MR imaging relaxation times of abdominal and pelvic tissues measured in vivo at 3.0 T: preliminary results. Radiology. 2004; 230(3):652–659. [PubMed: 14990831]
16. Feinberg DA, Hoenninger JC, Crooks LE, Kaufman L, Watts JC, Arakawa M. Inner volume MR imaging: technical concepts and their application. Radiology. 1985; 156(3):743–747. [PubMed: 4023236]
17. Semelka RC, Kelekis NL, Thomasson D, Brown MA, Laub GA. HASTE MR imaging: description of technique and preliminary results in the abdomen. J Magn Reson Imaging. 1996; 6(4):698–699. [PubMed: 8835965]
18. Maccotta L, Detre JA, Alsop DC. The efficiency of adiabatic inversion for perfusion imaging by arterial spin labeling. NMR Biomed. 1997; 10(4–5):216–221. [PubMed: 9430351]
19. Wu WC, Fernandez-Seara M, Detre JA, Wehrli FW, Wang J. A theoretical and experimental investigation of the tagging efficiency of pseudocontinuous arterial spin labeling. Magn Reson Med. 2007; 58(5):1020–1027. [PubMed: 17969096]
20. Moore JE Jr, Ku DN. Pulsatile velocity measurements in a model of the human abdominal aorta under resting conditions. J Biomech Eng. 1994; 116(3):337–346. [PubMed: 7799637]
21. Ferrara LA, Mancini M, Iannuzzi R, et al. Carotid diameter and blood flow velocities in cerebral circulation in hypertensive patients. Stroke. 1995; 26(3):418–421. [PubMed: 7886717]
22. Avants BB, Epstein CL, Grossman M, Gee JC. Symmetric diffeomorphic image registration with cross-correlation: evaluating automated labeling of elderly and neurodegenerative brain. Med Image Anal. 2008; 12(1):26–41. [PubMed: 17659998]
23. Shao, X., Tisdall, MD., Wang, DJ., van der Kouwe, AJ. Prospective motion correction for 3D GRASE pCASL with volumetric navigators. International Society for Magnetic Resonance in Medicine; 2017. p. 0680
24. Wang DJ, Alger JR, Qiao JX, et al. Multi-delay multi-parametric arterial spin-labeled perfusion MRI in acute ischemic stroke - Comparison with dynamic susceptibility contrast enhanced perfusion imaging. Neuroimage Clin. 2013; 3:1–7. [PubMed: 24159561]
25. Lu H, Clingman C, Golay X, van Zijl PC. Determining the longitudinal relaxation time (T1) of blood at 3.0 Tesla. Magn Reson Med. 2004; 52(3):679–682. [PubMed: 15334591]
26. Dai W, Robson PM, Shankaranarayanan A, Alsop DC. Reduced resolution transit delay prescan for quantitative continuous arterial spin labeling perfusion imaging. Magn Reson Med. 2012; 67(5): 1252–1265. [PubMed: 22084006]
27. Bower S, Vyas S, Campbell S, Nicolaides KH. Color Doppler imaging of the uterine artery in pregnancy: normal ranges of impedance to blood flow, mean velocity and volume of flow. Ultrasound Obstet Gynecol. 1992; 2(4):261–265. [PubMed: 12796952]
28. Zun Z, Shankaranarayanan A, Bulas D, Du Plessis AJ, Limperopoulos C. Three-dimensional placental perfusion imaging using velocity-selective arterial spin labeled Mri: Preliminary results. Prenatal Diagnosis. 2015; 35:3–4.
29. Sorensen A, Sinding M, Peters DA, et al. Placental oxygen transport estimated by the hyperoxic placental BOLD MRI response. Physiol Rep. 2015; 3(10)
30. Ingram E, Hawkins L, Morris DM, et al. R1 changes in the human placenta at 3 T in response to a maternal oxygen challenge protocol. Placenta. 2016; 39:151–153. [PubMed: 26992688]
31. Konje JC, Kaufmann P, Bell SC, Taylor DJ. A longitudinal study of quantitative uterine blood flow with the use of color power angiography in appropriate for gestational age pregnancies. Am J Obstet Gynecol. 2001; 185(3):608–613. [PubMed: 11568786]
32. Baker PN, Johnson IR, Harvey PR, Gowland PA, Mansfield P. A three-year follow-up of children imaged in utero with echo-planar magnetic resonance. Am J Obstet Gynecol. 1994; 170(1 Pt 1): 32–33. [PubMed: 8296840]
33. Choi JS, Ahn HK, Han JY, et al. A case series of 15 women inadvertently exposed to magnetic resonance imaging in the first trimester of pregnancy. J Obstet Gynaecol. 2015; 35(8):871–872. [PubMed: 26033169]
34. Hand JW, Li Y, Hajnal JV. Numerical study of RF exposure and the resulting temperature rise in the foetus during a magnetic resonance procedure. Phys Med Biol. 2010; 55(4):913–930. [PubMed: 20090188]

35. Glover P, Hykin J, Gowland P, Wright J, Johnson I, Mansfield P. An assessment of the intrauterine sound intensity level during obstetric echo-planar magnetic resonance imaging. Br J Radiol. 1995; 68(814):1090–1094. [PubMed: 7496710]

36. Reeves MJ, Brandreth M, Whitby EH, et al. Neonatal cochlear function: measurement after exposure to acoustic noise during in utero MR imaging. Radiology. 2010; 257(3):802–809. [PubMed: 20876389]

37. Hattori Y, Fukatsu H, Ishigaki T. Measurement and evaluation of the acoustic noise of a 3 Tesla MR scanner. Nagoya J Med Sci. 2007; 69(1–2):23–28. [PubMed: 17378177]

38. Williams DS, Detre JA, Leigh JS, Koretsky AP. Magnetic resonance imaging of perfusion using spin inversion of arterial water. Proc Natl Acad Sci U S A. 1992; 89(1):212–216. [PubMed: 1729691]

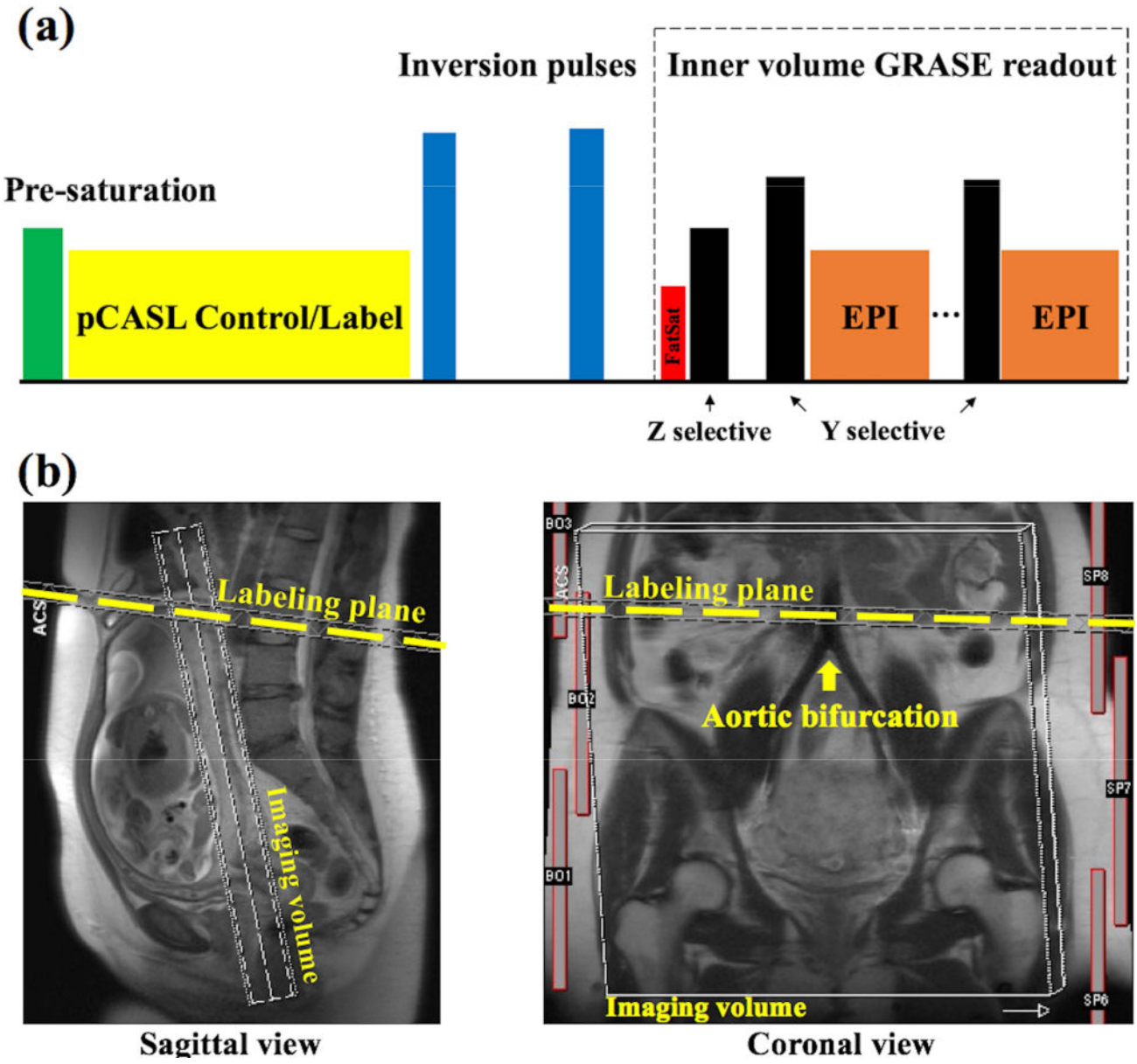

Figure 1.

(a) Scheme of inner-volume GRASE pCASL sequence. Background suppression was achieved by two inversion pulses following a whole volume pre-saturation. Switching the slice selective gradient to Y-axis for re-focusing pulses preserved the signal only within the targeting imaging volume to avoid wrapping around artifacts along Y-axis. (b) Demonstration of spatial position of imaging volume and ASL labeling plane. Labeling place was placed at aortic bifurcation and highlighted by the yellow dashed line.

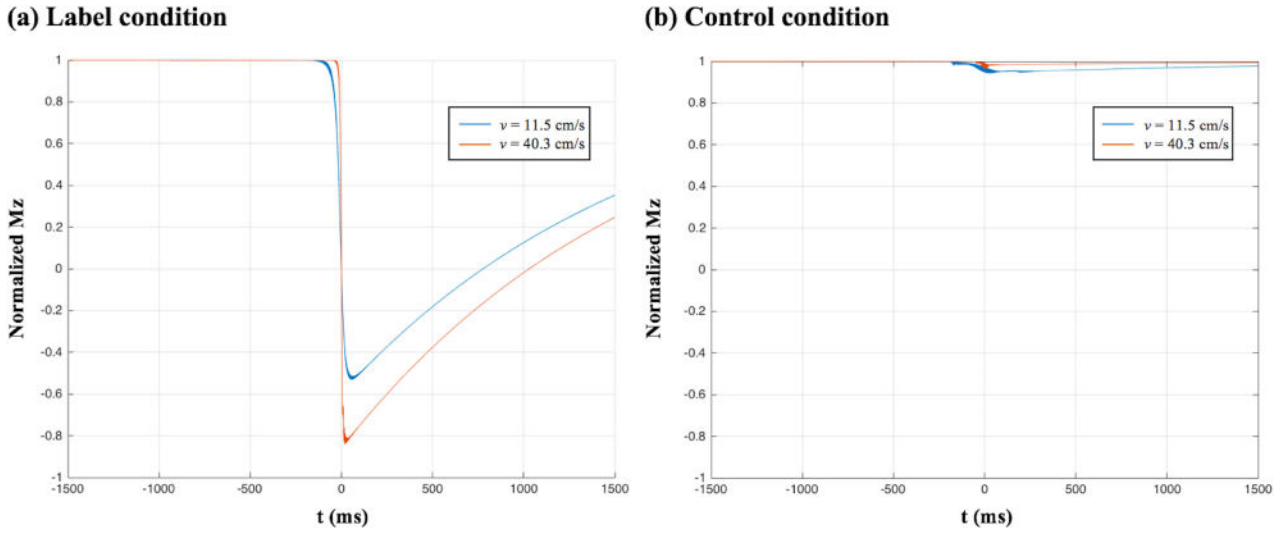

Figure 2.

Simulated time courses of longitudinal magnetization of spins moving across the labeling plane (t=0 ms) under: (a) label and (b) control conditions. Velocities of spins are 11.5 cm/s and 40.3 cm/s, which represent the vessel center velocity at aortic bifurcation and carotid arteries, respectively.

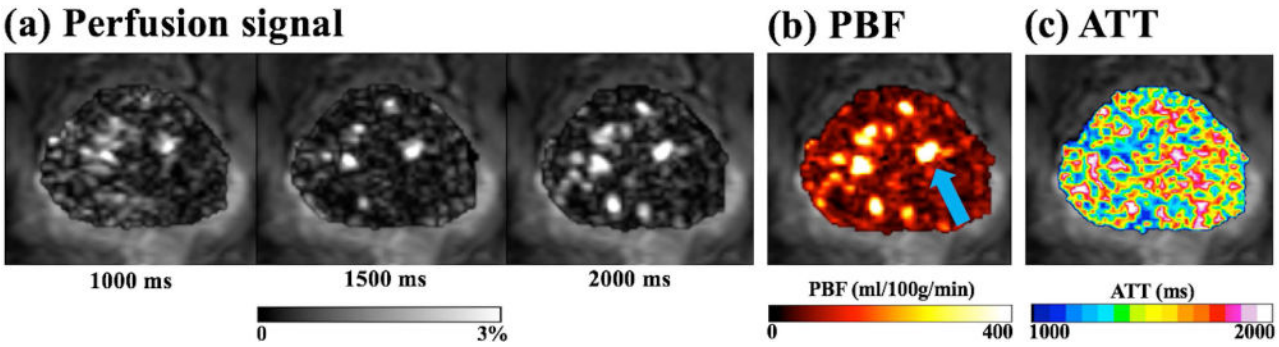

Figure 3.

(a) Perfusion signal at PLD 1000/1500/2000 ms of a representative slice. (b) Calculated PBF maps. One of focal hyper-perfusion regions was indicated by a blue arrow. (c) Calculated ATT maps. Images are overlaid on the T2-weighted structural image measured by GRASE sequence.

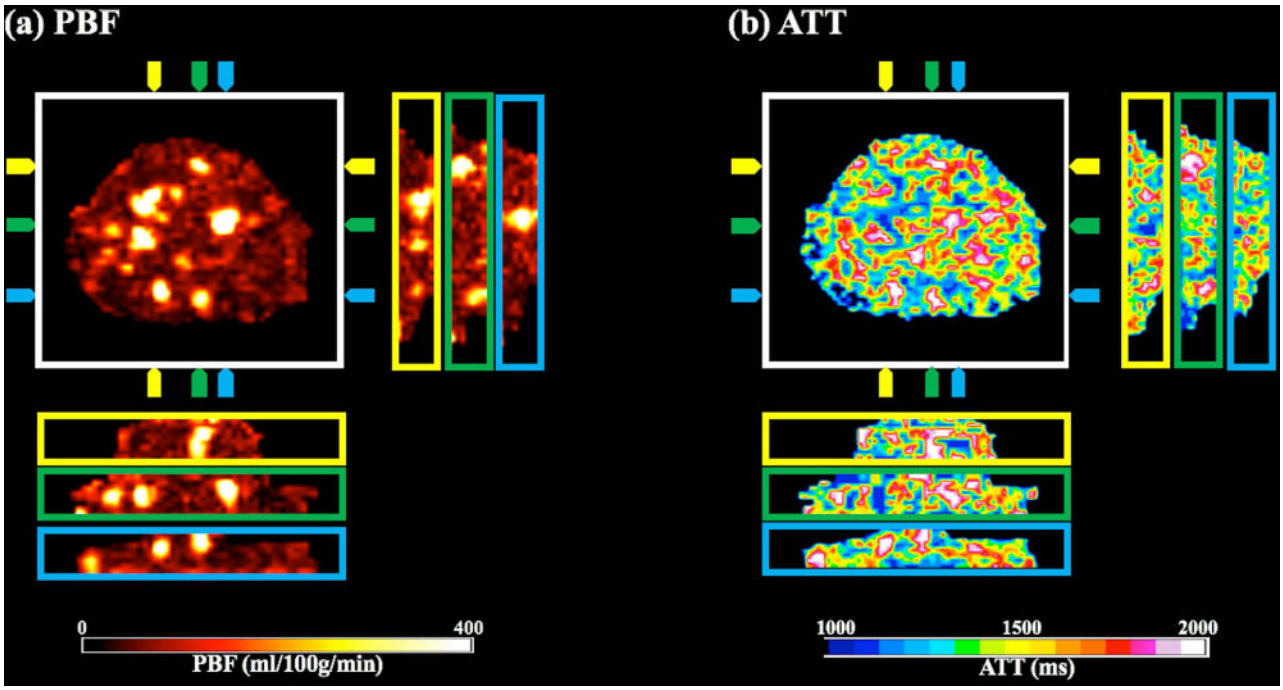

Figure 4.

3D views of PBF (a) and ATT (b) map. Three pairs of coronal/sagittal slices were displayed adjacent to the transverse plane, and their spatial positions were specified by color arrows around the transverse image.

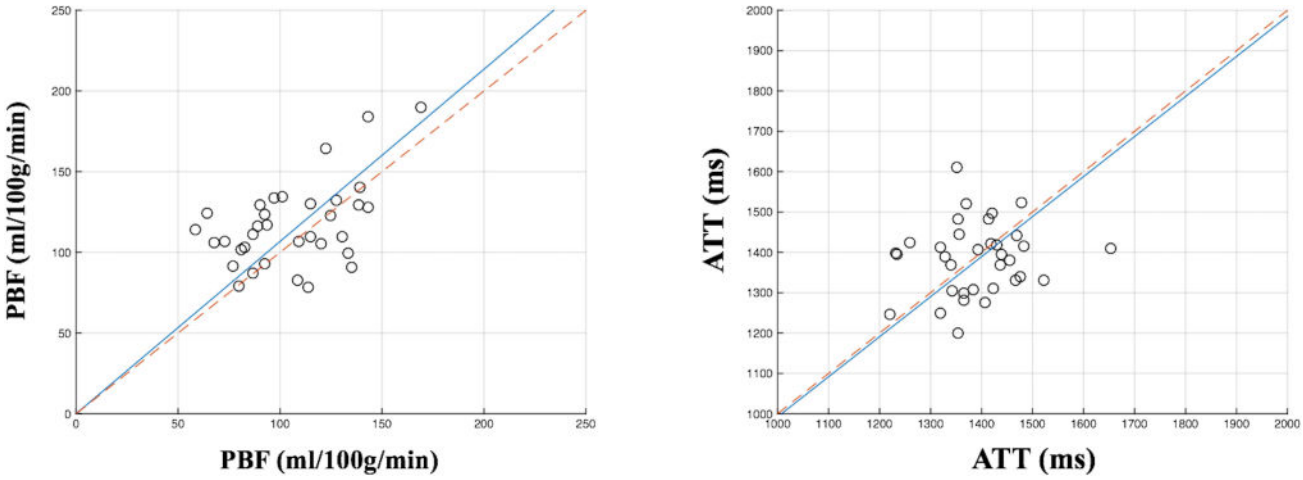

Figure 5.

Comparison of PBF (left plot) and ATT (right plot) acquired from two scans within the second trimester. Each dot in the plot represents PBF or ATT of a single subject while horizontal and vertical axes represent the data from the first (14–16 weeks) and second (19–22 weeks) scans respectively. Slope of the solid blue line was estimated from 34 subjects' data using the least square method. Red dashed line was plotted for reference with a slope of 1 indicating no change between two scans.

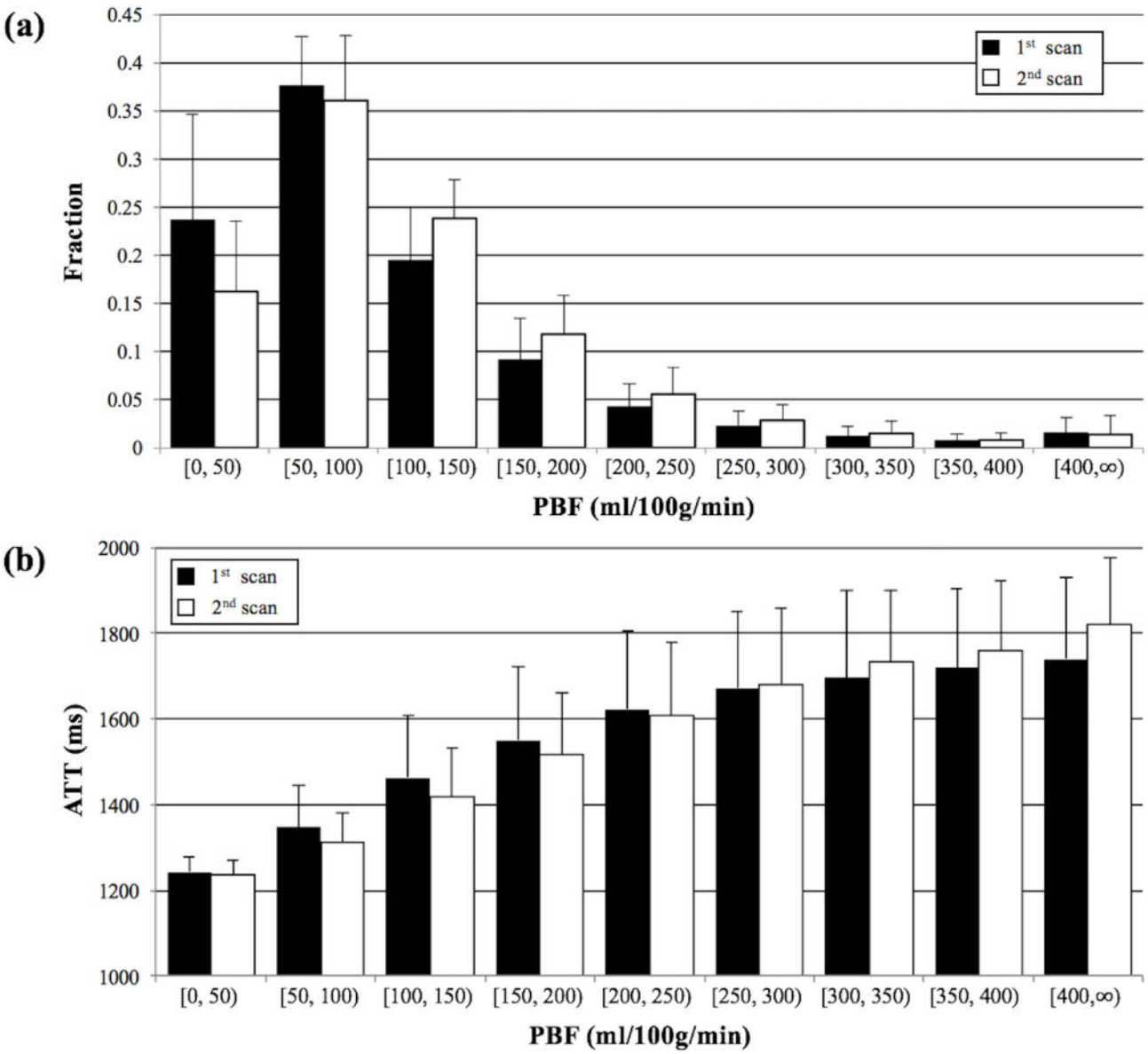

Figure 6.

(a) Histogram of PBF values, which was divided into nine consecutive bins with a width of 50 ml/100g/min except the last bin is open ended, at repeated scans. Fraction of PBF values in each bin was averaged across 34 subjects with error bars indicating the inter-subject standard deviation. (b) Mean ATT in nine regions corresponding to PBF bins at repeated scans. Each bar represented the ATT averaged across 34 subjects with error bars indicating the inter-subject standard deviation.

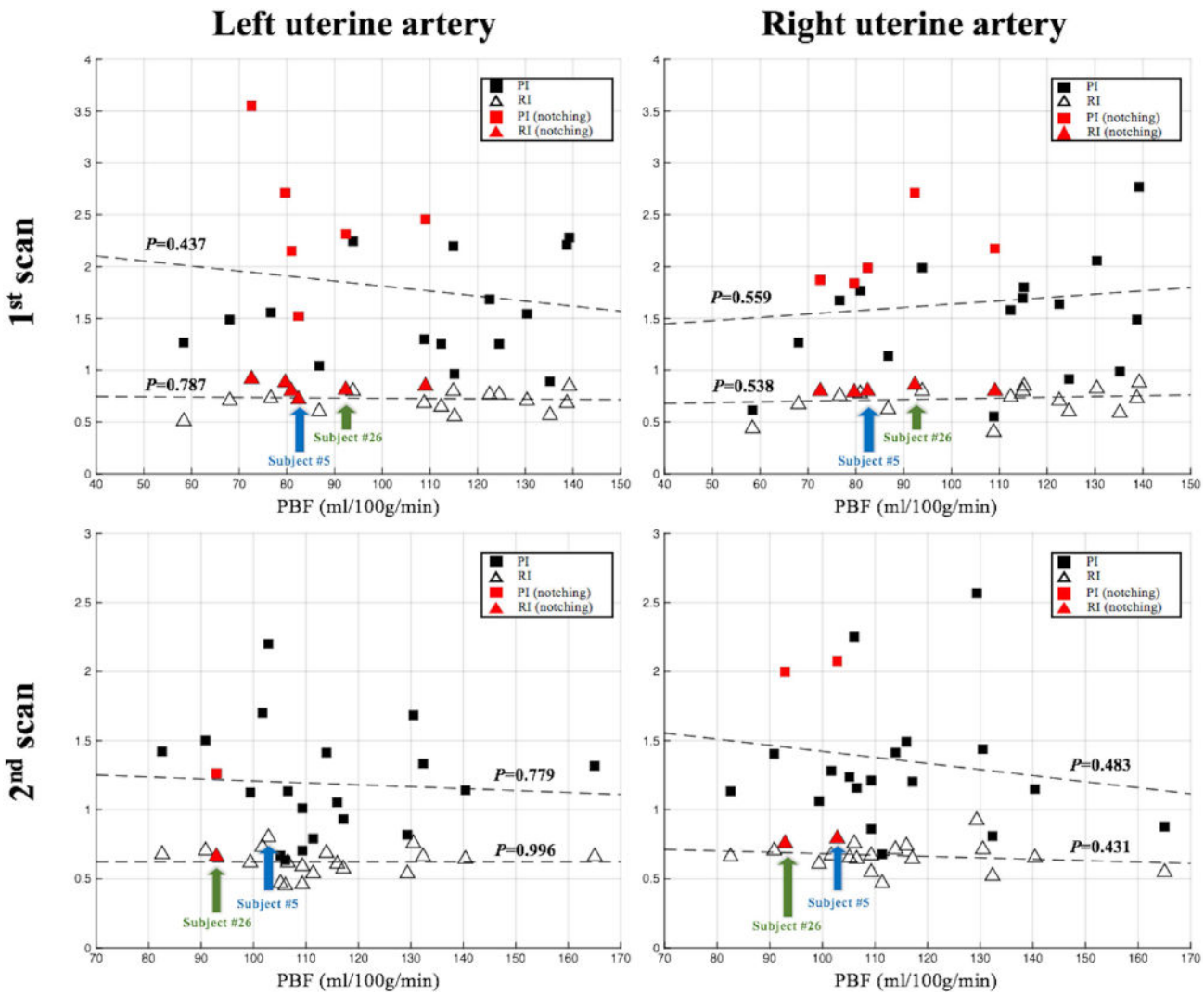

Figure 7.

Scatter plot of resistance index (RI) and pulsatility index (PI) versus PBF values. Left and right column showed RI/PI from left and right uterine artery, respectively. Top and bottom row showed results acquired after the first and second MRI scans, respectively. Linear regression between RI/PI and PBF was illustrated by dashed lines, and no significant correlation was found (*P* values were listed next to each dashed line). Subjects with the early diastolic notch were labeled by red filled marks. Bilateral/unilateral notches presented in three/one subjects' Doppler ultrasound waveform pattern acquired after the first MRI scan. Two subjects (subject #5 and #26) with persistent notches at two scans were identified by blue and green arrows. Bilateral/unilateral notches presented in subject #26/#5 Doppler ultrasound waveform pattern acquired after the second MRI scan.

Table 1

Summary of PBF and ATT from the first group (14–16 weeks), the second group (19–22 weeks) and the overall average.

	PBF (ml/100g/min)	ATT (ms)
14–16 weeks	105.9±26.5	1390.4±86.9
19–22 weeks	116.9±25.7	1384.5±87.6
All subjects	111.4±26.7	1387.5±88.0